Journal of Alloys and Compounds 509 (2011) 9770–9775

Contents lists available at ScienceDirect

Journal of Alloys and Compounds

journal homepage: www.elsevier.com/locate/jallcom

Modification of TiO_2 nanorods by Bi_2MoO_6 nanoparticles for high performance visible-light photocatalysis

Na Li, Li Zhu, Wei-De Zhang*, Yu-Xiang Yu, Wen-Hui Zhang, Mei-Fang Hou

School of Chemistry and Chemical Engineering, South China University of Technology, 381 Wushan Road, Guangzhou 510640, People's Republic of China

ARTICLE INFO

Article history:
Received 12 April 2011
Received in revised form 8 July 2011
Accepted 30 July 2011
Available online 4 August 2011

Keywords:
Nanostructured composites
Bi_2MoO_6/TiO_2
Bi_2MoO_6 nanoparticles
TiO_2 nanorods
Photocatalytic activity

ABSTRACT

In this work, TiO_2 nanorods were prepared by a hydrothermal process and then Bi_2MoO_6 nanoparticles were deposited onto the TiO_2 nanorods by a solvothermal process. The nanostructured Bi_2MoO_6/TiO_2 composites were extensively characterized by X-ray diffraction, scanning and transmission electron microscopy, X-ray photoelectron spectroscopy and UV–vis diffuse reflectance spectroscopy. The photocatalytic activity of the Bi_2MoO_6/TiO_2 composites was evaluated by degradation of methylene blue. The Bi_2MoO_6/TiO_2 composites exhibit higher catalytic activity than pure Bi_2MoO_6 and TiO_2 for degradation of methylene blue under visible light irradiation ($\lambda > 420$ nm). Further investigation revealed that the ratio of Bi_2MoO_6 to TiO_2 in the composites greatly influenced their photocatalytic activity. The experimental results indicated that the composite with Bi_2MoO_6:TiO_2 = 1:3 exhibited the highest photocatalytic activity. The enhancement mechanism of the composite catalysts was also discussed.

1. Introduction

In recent years, because of the extensive use of dyes, the organic dye pollutants in liquid waste have become one of the main pollutants in wastewater. To resolve this problem, besides other well-established techniques, the method based on semiconductor photocatalysts is a promising solution to degrade organic pollutants in waste water [1]. Among the various semiconductor photocatalysts, TiO_2 has been extensively investigated and proved to be the most effective photacatalyst for degradation of organic pollutants because of its low cost, non-toxicity, high activity and stability to photo or chemical corrosion [2–6]. However, as it is known to all, TiO_2 is a semiconductor with wide band gap (3.18 eV for anatase and 3.02 eV for rutile) and relatively high rate of photogenerated electron–hole recombination. TiO_2 only responds to ultraviolet irradiation but not to visible light that accounts for 43% of the incoming solar energy [7,8] and has low quantum efficiency. To overcome the two drawbacks, a heap of studies have been carried out over the past decades to develop modified TiO_2 in order to make it active under visible-light. Two main approaches have been applied. One is to dope TiO_2 with foreign ions, including metal and nonmetal elements, such as N-doped TiO_2 [9], C-doped TiO_2 [10], Bi^{3+}-doped TiO_2 [11], C, Cl-codoped TiO_2 [12], Cu, S-codoped TiO_2 [13] and so on. Because of forming a relatively narrow band between TiO_2 and the foreign ions, this method can indeed extend the absorption region of TiO_2 to visible light. However, the metal elements-doped TiO_2 shows weaker oxidation ability and the less mobility of photogenerated holes in the relatively narrow band than those in the valence band (VB) of TiO_2 [14]. Moreover, the doped TiO_2 cannot absorb sufficient visible light and massive charge carriers inevitably recombine [15]. So, these photocatalysts typically cannot exhibit the same activity under UV light as under visible light. That means the doping of foreign elements into TiO_2 is not a perfect approach to develop TiO_2 photocatalysts sensitive to visible light [16]. Another method is to combine TiO_2 with other narrow band gap semiconductors to form composite photocatalysts. In the composite photocatalysts, the narrow band gap semiconductors can be excited under visible light irradiation. With the matching band potentials, the photogenerated electrons or holes will then be transferred to TiO_2, which leads to efficient charge separation and enhances photocatalytic ability. Recently, some novel photocatalysts based on semiconductor composites, for example, coupling TiO_2 with CdS [17], Cr_2O_3–CNT [18] and SnO_2 [19] have been developed, which are not only visible light active but also with improved quantum efficiency. Modification of TiO_2 by other narrow band gap semiconductors could be an effective way to extend the photoabsorption range and facilitate the separation of the photoinduced carriers [8].

As a new photocatalyst, Bi_2MoO_6 has attracted considerable attention recently. Its band gap is 2.71 eV, so it can absorb visible light with an absorbance wavelength of 490 nm. Moreover, it can thoroughly decompose dye pollutants to inorganic compounds. Its band positions ($E_{CB} = -0.32$ eV, $E_{VB} = 2.39$ eV) are in

* Corresponding author. Tel.: +86 20 8711 4099; fax: +86 20 8711 4099.
E-mail address: zhangwd@scut.edu.cn (W.-D. Zhang).

0925-8388/$ – see front matter © 2011 Elsevier B.V. All rights reserved.
doi:10.1016/j.jallcom.2011.07.102

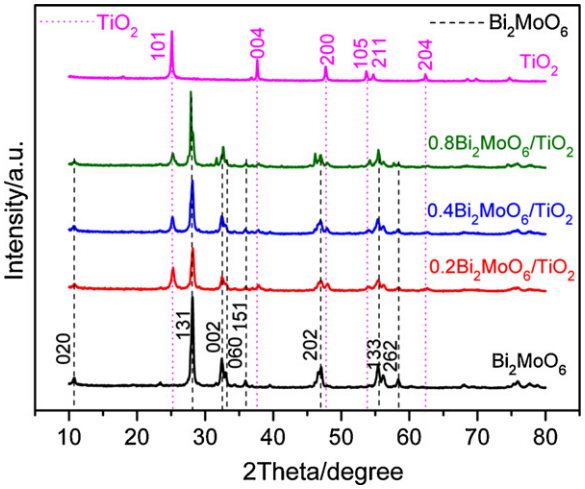

Fig. 1. XRD patterns of the as-prepared TiO_2 nanorods, Bi_2MoO_6/TiO_2 composites and Bi_2MoO_6 nanoparticles.

good alignment with those of TiO_2 ($E_{CB} = -0.29$ eV, $E_{VB} = 2.91$ eV) to form a heterojunction photocatalyst. Therefore, modification of TiO_2 by Bi_2MoO_6 is promising to endow the composite catalysts with enhanced photocatalytic activity. Herein, for the first time, we report the modification of TiO_2 nanorods by Bi_2MoO_6 nanoparticles as a visible light responsive photocatalyst, which exhibits excellent visible-light-driven photocatalytic activity for the degradation of methylene blue (MB), a common model pollutant in wastewater. Owing to the synergistic effect of Bi_2MoO_6 and TiO_2, the composites also show enhanced photocatalytic activity under visible-light irradiation. The results reported in this study also provide insight to construct other composite photocatalysts.

2. Experimental

2.1. Preparation of Bi_2MoO_6/TiO_2

All chemicals were of analytical grade and purchased from local chemical agents without further purification. Anatase TiO_2 nanorods were synthesized by hydrothermal reaction according to Ref. [20]: 1.0 g commercial TiO_2 was added into a 50 mL Teflon vessel then filled with 10 M NaOH aqueous solution up to 80% of the total volume. The Teflon-lined autoclave was heated up to 200 °C and then maintained for 24 h. After cooling down naturally, the product was centrifuged, washed and dried. The obtained product was immerged into a 0.1 M HNO_3 solution for 6 h, washed until the pH of the solution to be about 7, and then dried at 60 °C for 12 h to get H-titanate nanofibers. The obtained H-titanate nanofibers were added into a 100 mL Teflon vessel then filled with dilute HNO_3 aqueous solution (pH = 2) up to 80% of the total volume and maintained at 180 °C for 24 h. Finally, the product was isolated from the solution by centrifugation and sequentially washed with deionized water for several times, and dried at 60 °C for 12 h.

In order to deposit Bi_2MoO_6 nanoparticles onto TiO_2 nanorods, the starting materials, $Bi(NO_3)_3{\cdot}5H_2O$ and $(NH_4)_6Mo_7O_{24}{\cdot}4H_2O$ with molar ratio (Bi/Mo) of 2:1 were dissolved in diethylene glycol. Then, 1.2 mmol TiO_2 nanorods and various doses of the above solution with desired amount of the precursors to corresponding amount of Bi_2MoO_6 (0.2 mmol, 0.4 mmol, 0.8 mmol) were added into the Teflon-lined autoclave. The hydrothermal reaction was carried out at 160 °C for 12 h. The product was isolated from the solution by centrifugation and thoroughly washed with deionized water and ethanol to remove any ionic residual, and then dried in an oven at 60 °C for 12 h for further characterization.

For comparison, the pure TiO_2 nanorods and Bi_2MoO_6 nanoparticles prepared via the same solvothermal process and the mechanical mixture of Bi_2MoO_6 nanoparticles and TiO_2 nanorods ($Bi_2MoO_6 + TiO_2$) by grinding in a mortar were also prepared.

2.2. Characterization

The morphology and crystal structure of the prepared samples were carefully characterized. The X-ray diffraction (XRD) patterns of the samples were recorded on a Bruker D8 Focus X-ray diffractometer with Cu Kα radiation (λ = 0.154184 nm). The morphologies and microstructures of the as-prepared samples were analyzed by scanning electron microscopy (SEM, JEOL JSM-6380-LA, Japan) and high-resolution transmission electron microscopy (HRTEM, FEI Tecnai F20). UV–vis diffuse reflectance spectra (DRS) were recorded on an UV–vis spectrophotometer (Hitachi U-3010) by using $BaSO_4$ as a reference in wavelength of 200–800 nm.

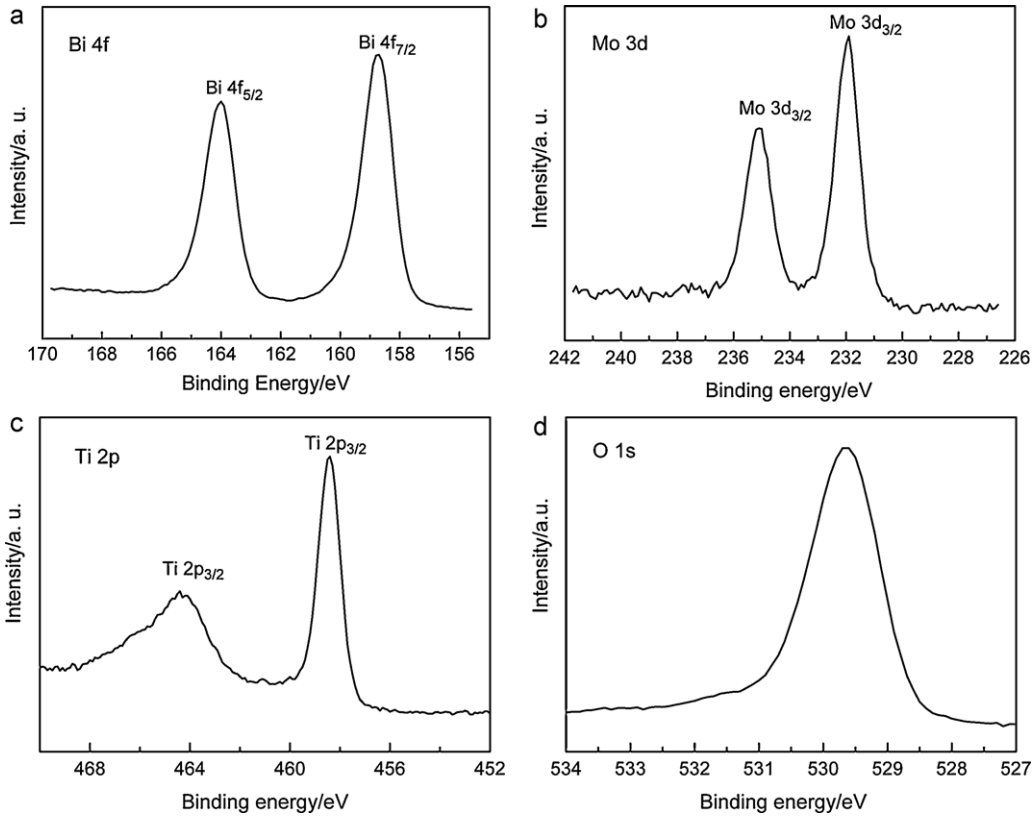

Fig. 2. XPS spectra of Bi 4f, Mo 3d, Ti 2p and O 1s of the $0.4Bi_2MoO_6/TiO_2$ composite.

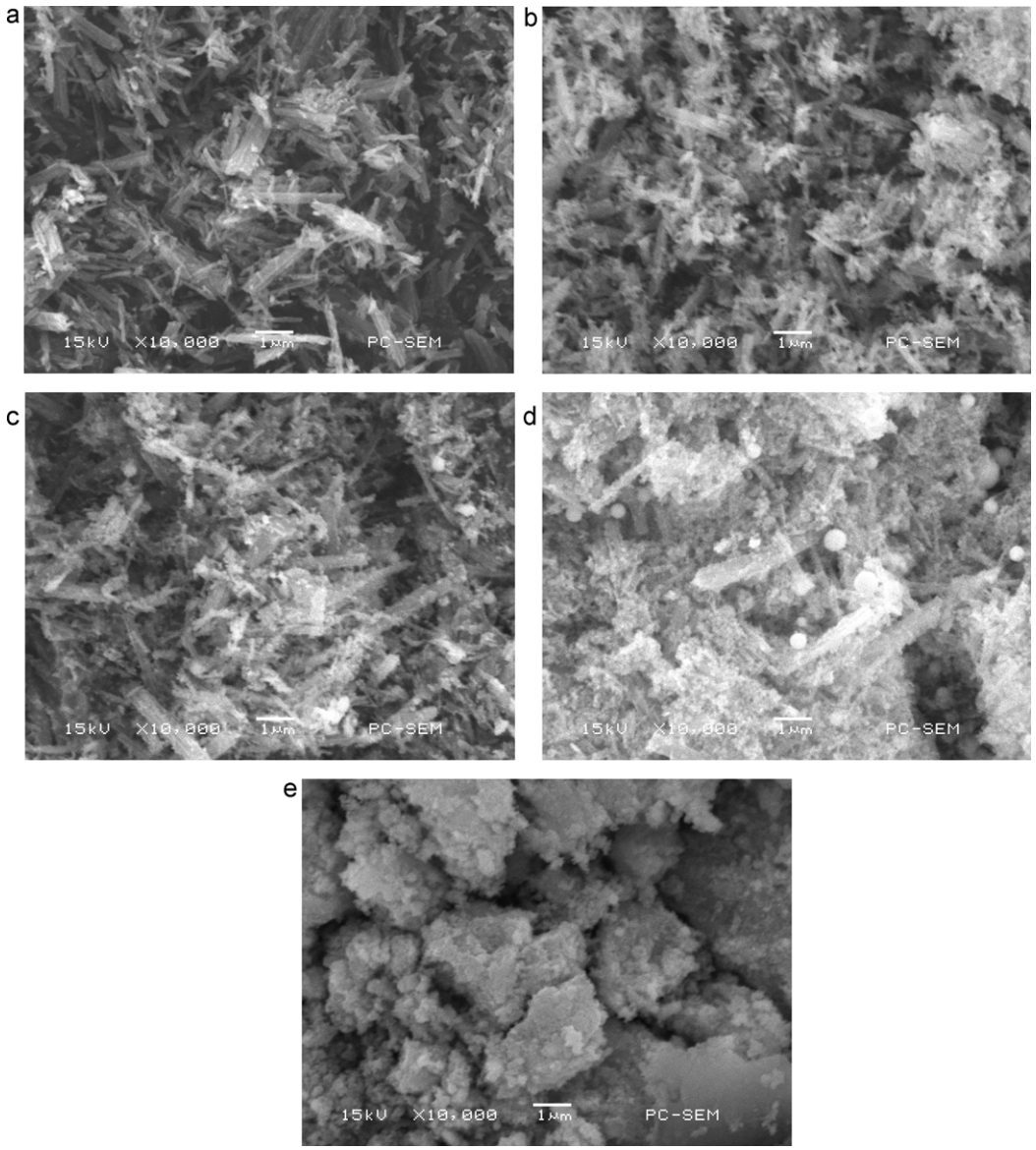

Fig. 3. SEM images of the prepared samples: (a) TiO_2 nanorods, (b) $0.2Bi_2MoO_6/TiO_2$, (c) $0.4Bi_2MoO_6/TiO_2$, (d) $0.8Bi_2MoO_6/TiO_2$ composites and (e) Bi_2MoO_6 nanoparticles.

The XPS spectra of the photocatalysts were measured on a Kratos Axis Ultra DLD photoelectron spectrometer.

2.3. Evaluation of photocatalytic activity

Methylene blue was chosen as the target pollutant for evaluating the photocatalytic activity of the catalysts, since it is a typical azo dye and difficult to degrade. A 400 W metal-halide lamp was used as the light source with a 420 nm cutoff filter to provide visible light irradiation. In a typical photocatalytic experiment, 0.10 g of the photocatalyst was dispersed in 150 mL MB solution (10^{-5} mol/L). Before visible light illumination, the suspensions were magnetically stirred in dark for 30 min to ensure the adsorption–desorption equilibrium of MB on the catalyst. Then, the solution was exposed to visible light irradiation under magnetic stirring. At given time intervals, 5 mL suspension was taken out and centrifuged to remove the photocatalyst powders. The concentration of MB was analyzed by a Hitachi U-3310 UV–vis spectrophotometer, and the absorbance at 664 nm was monitored.

3. Results and discussion

3.1. XRD analysis

The crystal structure and phase composition of the prepared TiO_2, Bi_2MoO_6 and Bi_2MoO_6/TiO_2 samples were characterized by X-ray diffraction, as shown in Fig. 1. The TiO_2 sample used as the substrate is composed of anatase crystal phase (Fig. 1a). The diffraction peaks at 2θ of 25.28°, 37.80°, 48.04°, 53.89°, 55.06° and 62.68° can be indexed to the characteristic peaks (1 0 1), (0 0 4), (2 0 0), (1 0 5), (2 1 1) and (2 0 4) of anatase TiO_2 (JCPDS 21-1272), respectively. The diffraction peaks at 2θ of 10.92°, 28.30°, 32.64°, 33.14°, 36.05°, 46.73°, 55.58° and 58.47° could be indexed to the characteristic peaks (0 2 0), (1 3 1), (0 0 2), (0 6 0), (1 5 1), (2 0 2), (1 3 3) and (2 6 2) of the orthorhombic structure of Bi_2MoO_6, respectively (Fig. 1f). All the peaks can be well indexed to the orthorhombic structure of Bi_2MoO_6 with lattice constants of $a = 0.550$ nm, $b = 1.621$ nm, and $c = 0.548$ nm, which is in good agreement with the standard data (JCPDS 21-0102). Moreover, all of the diffraction peaks of the Bi_2MoO_6/TiO_2 samples can be indexed as well-crystallized orthorhombic Bi_2MoO_6 (JCPDS 21-0102) and anatase TiO_2 (Fig. 1b–e). Furthermore, it can be observed that with the increase of Bi_2MoO_6 to TiO_2 ratio, the diffraction peaks of Bi_2MoO_6 are stronger but the peaks of TiO_2 become weaker. Compared with Fig. 1f, the peaks corresponding to orthorhombic Bi_2MoO_6 in Fig. 1b–e become broader, which means that the size of Bi_2MoO_6 becomes smaller. This result will be further testified by SEM obser-

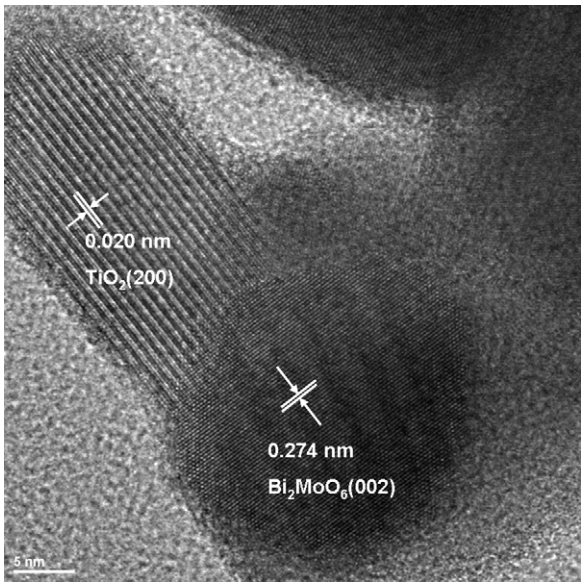

Fig. 4. HRTEM image of the $0.4Bi_2MoO_6/TiO_2$ nanocomposite.

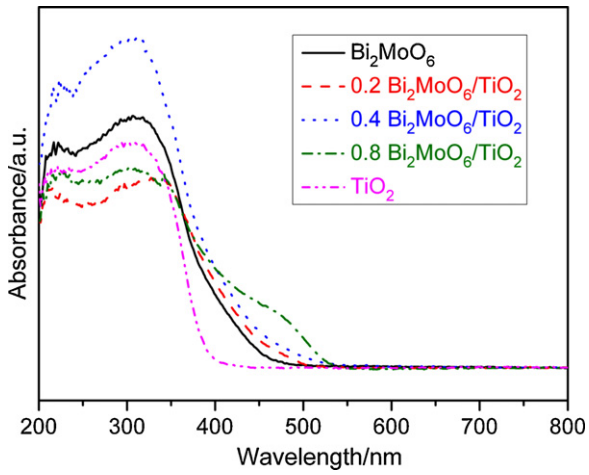

Fig. 5. UV–vis diffuse reflectance spectra of the prepared samples.

vation. Therefore, it can be concluded that the introduction of TiO_2 inhibits the Bi_2MoO_6 nanoparticles from growing bigger, which may be caused by heterostructural formation between Bi_2MoO_6 and TiO_2 nanocrystals in the composites [1,21].

3.2. XPS analysis

To determine the chemical composition of the Bi_2MoO_6/TiO_2 composites, XPS analysis was carried out. Fig. 2 illustrates the XPS spectra of Bi 4f, Mo 3d and Ti 2p. The two peaks at 164.0 and 158.7 eV are assigned to Bi $4f_{5/2}$ and Bi $4f_{7/2}$, respectively (Fig. 2a), corresponding to Bi^{3+} [22]. The two strong peaks at 235.1 and 231.9 eV in Fig. 2b can be assigned to Mo $3d_{1/2}$ and Mo $3d_{3/2}$, respectively, demonstrating that the main chemical state of Mo in the composite is Mo^{6+} [23]. The binding energy of TiO_2 was obtained at 458.4 and 464.4 eV, corresponding to Ti $2p_{3/2}$ and Ti $2p_{1/2}$, respectively, which is the same as the pure TiO_2 photocatalyst [24,25]. In summary, from the XPS analysis, all of the elements expected appeared. No doped phenomenon in the composite was observed.

3.3. SEM and TEM observation

The morphology and crystal structure of the Bi_2MoO_6/TiO_2 composites were further observed by SEM and TEM. As shown in Fig. 3, it can be obviously observed that Bi_2MoO_6 nanoparticles are successfully attached onto the TiO_2 nanorods. Furthermore, it is clear from SEM images that the nanoparticles in the Bi_2MoO_6/TiO_2 composites are decentralized very well than pure Bi_2MoO_6 ones. With increasing Bi_2MoO_6 loading level, some bigger particles were also found (Fig. 3c and d). During the deposition, the TiO_2 nanorods served as heterogeneous nuclei for the growth of Bi_2MoO_6, while the existence of TiO_2 nanorods also inhibit the growing up of Bi_2MoO_6 nanoparticles [1,26]. Further observation of the prepared sample by HRTEM reveals that the Bi_2MoO_6 nanoparticles are not just loosely attached to the nanorods surface but rooted inside the TiO_2 nanorods (Fig. 4). The HRTEM observation demonstrates two sets of different fringes. The lattice fringe of 0.190 nm corresponds to the (2 0 0) crystal plane of an anatase structure of TiO_2, while the fringe of 0.274 nm matches well with the (0 0 2) plane of Bi_2MoO_6. The well-defined fringes and the high crystalline of the Bi_2MoO_6/TiO_2 composites facilitate the separation of the photoinduced carrier, which is beneficial for improving the corresponding photocatalytic activity [8].

3.4. Optical absorption property

The UV–vis diffuse reflectance spectra of the photocatalysts are shown in Fig. 5. From the typical diffuse absorption spectra, TiO_2 displays photoabsorption property in the UV light region, with an absorption edge at about 400 nm, while Bi_2MoO_6 has broader absorption in the visible region with an absorption edge of about 460 nm. Moreover, the plot of $(ah\nu)^{1/2}$ versus the energy of light [27] afforded band gap energy of 3.10 eV for TiO_2 and 2.70 eV for Bi_2MoO_6. However, it is noted that the absorption edge of the Bi_2MoO_6/TiO_2 composites shifts to longer wave (from 460 nm to 550 nm), and the red-shift increases upon the increase of Bi_2MoO_6. This can be attributed to the interaction of TiO_2 and Bi_2MoO_6 [6,28]. Large quantities of semiconductor with narrow band gap, that is, Bi_2MoO_6 in the Bi_2MoO_6/TiO_2 composites can result in stronger photosensitization and larger red-shift of the absorption edge.

3.5. Photocatalytic activity

In order to prove the enhanced photocatalytic activity of the nanostructured Bi_2MoO_6/TiO_2 composites compared with Bi_2MoO_6 nanoparticles, TiO_2 nanorods as well as mechanically mixed Bi_2MoO_6 nanoparticles and TiO_2 nanorods ($Bi_2MoO_6 + TiO_2$), the photocatalytic degradation of methyl blue under visible light irradiation was carried out. As a kind of typical organic dye, MB is chemically stable and difficult to be decomposed. The absorption of MB at the wavelength of 664 nm was monitored. Fig. 6 shows the photocatalytic degradation rate over different photocatalysts, where C_0 is the concentration of MB after the adsorption equilibrium on the samples in dark. Compared with the pure Bi_2MoO_6, TiO_2 and $Bi_2MoO_6 + TiO_2$, the composites show higher photocatalytic activity toward degradation of MB under visible light irradiation. As can be seen, the photodegradation of MB over TiO_2 was very limited because TiO_2 was not excitated under visible illumination. Though Bi_2MoO_6 can be excitated under visible illumination, the photodegradation of MB over the pure Bi_2MoO_6 is also almost negligible compared with the Bi_2MoO_6/TiO_2 composites. The reason is that photoinduced electrons and holes will recombine quickly on the surface of Bi_2MoO_6. Furthermore, when the TiO_2 nanorods were mixed with Bi_2MoO_6 nanoparticles mechanically, the photocatalytic activity was not enhanced because the heterostructure was difficult to form in such case. One point emerges with stark clarity from all we have said: the

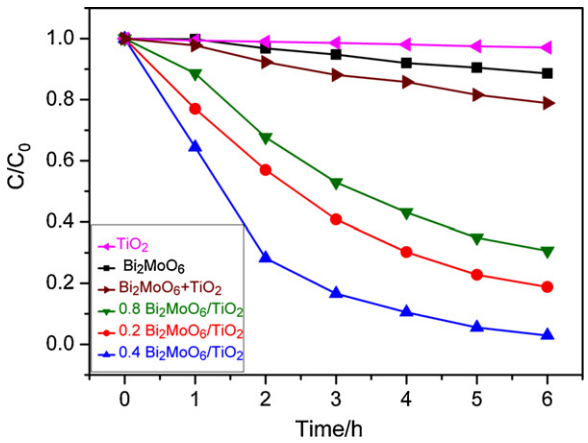

Fig. 6. Photodegradation of MB by using the prepared photocatalysts under visible light.

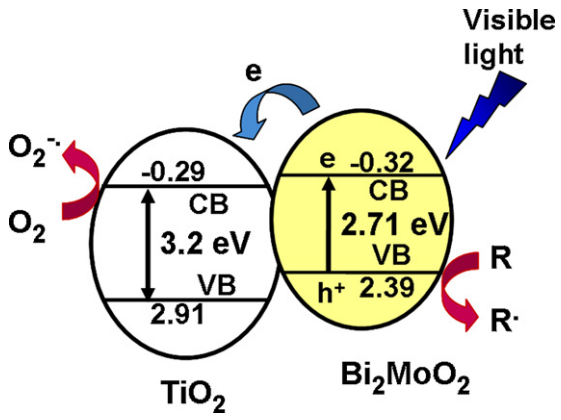

Fig. 8. Scheme diagram of the band levels of the Bi_2MoO_6/TiO_2 heterojunction and the possible reaction mechanism of the photocatalytic reactions.

heterostructure plays an important role in improving the photocatalytic activity. It is also observed that the loading amounts of Bi_2MoO_6 in the Bi_2MoO_6/TiO_2 composites play a crucial rule in the photocatalytic activity. A small amount of Bi_2MoO_6 on the TiO_2 nanorods leads to a sharp increase of MB degradation. The photocatalytic activity increased upon the increase of the Bi_2MoO_6 in the composite catalysts. The reason is that the existence of TiO_2 can facilitate the transfer of the photoinduced carriers so the recombination of photoinduced carriers can be suppressed and the photocatalytic properties will be improved. However, the photocatalytic activity decreased when the Bi_2MoO_6 amount continued rising. Upon the increase of Bi_2MoO_6 in the Bi_2MoO_6/TiO_2 composites, the photoinduced electrons and holes produced in Bi_2MoO_6 cannot efficiently transfer to the TiO_2 and they will recombine inevitably, thus decreasing the activity of the catalysts [8]. The experimental result reveals that the $0.4Bi_2MoO_6/TiO_2$ shows the optimal photocatalytic activity, with nearly 100% degradation of MB after 6 h visible-light irradiation.

Fig. 7 shows the temporal evolution of the spectral changes of MB solution in the photodegradation process over $0.4Bi_2MoO_6/TiO_2$ under visible light illumination ($\lambda > 420$ nm). It can be seen that the maximum absorption peak gradually decreased with irradiation time. After illumination for 6 h, both of the absorption peaks at 291 nm and 664 nm are very weak. Meanwhile, it is observed that the color of the MB solution almost changed from blue to colorless after visible light illumination

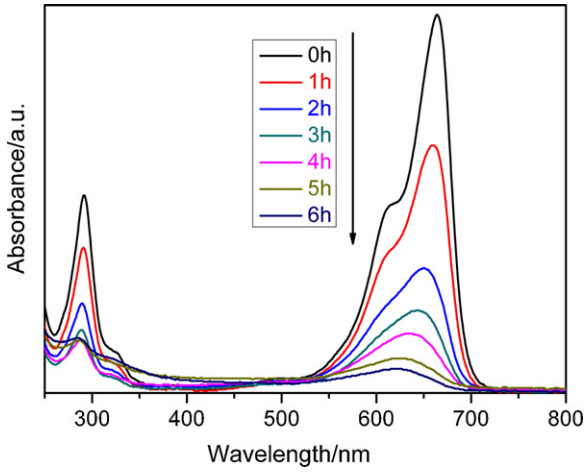

Fig. 7. Time-dependent UV–vis spectra of MB over the $0.4Bi_2MoO_6/TiO_2$ photocatalyst.

for 6 h, indicating a nearly complete degradation of MB. It is also clearly found that the spectral maximum shifted toward the blue region (from 664 to 621 nm) as reaction time went on. The blue-shift of the major absorption peak corresponds to a step-by-step N-demethylation of MB [29]. As a result, it confirms that MB was truly photodegraded by the Bi_2MoO_6/TiO_2 composites. The enhanced photocatalytic activity of the Bi_2MoO_6/TiO_2 composites can be ascribed to two main reasons: firstly, attachment of Bi_2MoO_6 nanoparticles onto TiO_2 nanorods improves their dispersion and inhibits their aggregation, which can be found from SEM observation. When the Bi_2MoO_6 nanoparticles disperse well, the contact between photocatalyst and dye molecules increases and the reaction efficiency will improve. More importantly, in the Bi_2MoO_6/TiO_2 composites, because Bi_2MoO_6 and TiO_2 have matching band potentials, the transfer of the photoinduced carriers was facilitated, thus improved the corresponding photocatalytic properties. When the Bi_2MoO_6/TiO_2 composite is under visible light irradiation, electrons (e^-) are excited to the conduction band of Bi_2MoO_6, leaving equal holes (h^+) in the valence band. Furthermore, the conduction band edge potential of TiO_2 is less negative than that of Bi_2MoO_6. Thus, electrons will transfer from the conduction band of Bi_2MoO_6 to TiO_2, which could react with electron acceptors such as O_2, reducing it to superoxide radical anion $O_2^{\bullet -}$ (Fig. 8). The anatase TiO_2 is used mainly as an electron-accepting semiconductor and Bi_2MoO_6 as a hole-holding semiconductor which has a strong oxidation potential and the holes consequently degrade the MB effectively [21,30]. As a result, the Bi_2MoO_6/TiO_2 composites showed much better photocatalytic activities than the pure Bi_2MoO_6. However, with increasing Bi_2MoO_6 in the Bi_2MoO_6/TiO_2 composites, there was an appropriate value, over which more photoinduced electrons and holes would recombine in Bi_2MoO_6, thus the photocatalytic activity would decrease. The optimal photocatalytic activity is obtained with the $0.4Bi_2MoO_6/TiO_2$, which is also coincident with its longest absorption edge.

4. Conclusions

We have demonstrated for the first time diethylene glycol-induced solvothermal synthesis of Bi_2MoO_6/TiO_2 composites via two-step hydrothermal process. The as-prepared Bi_2MoO_6/TiO_2 composites display enhanced visible light photocatalytic activity toward methylene blue, which has been greatly improved in comparison with pure Bi_2MoO_6 and TiO_2 nanorods. It is also found that the loading level of Bi_2MoO_6 in the Bi_2MoO_6/TiO_2 composites plays an important role in the photocatalytic property and the optimal ratio of Bi_2MoO_6 and TiO_2 is obtained at 1:3. The

dramatic enhancement in the visible light photocatalytic activity of the Bi_2MoO_6/TiO_2 composites can be mainly attributed to the efficient separation of photogenerated electron–hole pairs at the interface of the two semiconductors, which enhances the quantum efficiency. The experimental result proves that the Bi_2MoO_6/TiO_2 composites are effective photocatalysts under visible light irradiation. The present work not only provides an example of combining one semiconductor with another but also new insight to design nanostructured composites for catalysis.

Acknowledgment

The authors thank the National Natural Science Foundation of China (Nos. 21043005, 21003051 and No. 20773041) for financial support.

References

[1] Y.D. Liu, F. Xin, F. Wang, S.X. Luo, X.H. Yin, J. Alloys Compd. 498 (2010) 179.
[2] M.R. Hoffmann, S.T. Martin, W. Choi, D.W. Bahnemann, Chem. Rev. 95 (1995) 69.
[3] S.U.M. Khan, M. Al-Shahry, W.B. Ingler Jr., Science 297 (2002) 2243.
[4] A.L. Linsebigler, G.Q. Lu, J.T. Yates, Chem. Rev. 95 (1995) 735.
[5] G. Li, F. Liu, Z. Zhang, J. Alloys Compd. 493 (2010) L1.
[6] G.K. Zhang, X.M. Ding, F.S. He, X.Y. Yu, J. Zhou, Y.J. Hu, J.W. Xie, Langmuir 24 (2008) 1026.
[7] M.R. Hoffmann, S.T. Martin, W. Choi, D.W. Bahnemann, Chem. Rev. 95 (1995) 69–96.
[8] H.F. Cheng, B.B. Huang, Y. Dai, X.Y. Qin, X.Y. Zhang, Langmuir 26 (9) (2010) 6618.
[9] C. Burda, Y.B. Lou, X.B. Chen, A.C.S. Samia, J. Stout, J.L. Gole, Nano Lett. 3 (8) (2003) 1049.
[10] W.J. Ren, Z.H. Ai, F.L. Jia, L.Z. Zhang, X.X. Fan, Z.G. Zou, Appl. Catal. B 69 (2007) 138.
[11] J. Yu, S. Liu, Z. Xiu, W. Yu, G. Feng, J. Alloys Compd. 461 (2008) L17.
[12] H. Xu, L.Z. Zhang, J. Phys. Chem. C 114 (2010) 11534.
[13] M. Hamadanian, A. Reisi-Vanani, A. Majedi, Appl. Surf. Sci. 256 (2010) 1837.
[14] H. Irie, Y. Watanabe, K.J. Hashimoto, Phys. Chem. B 107 (2003) 5483.
[15] L. Zhou, M.M. Yu, J. Yang, Y.H. Wang, C.Z. Yu, J. Phys. Chem. C 114 (2010) 18812.
[16] H.G. Yu, H. Irie, Y. Shimodaira, Y. Hosogi, Y. Kuroda, M. Miyauchi, K. Hashimoto, J. Phys. Chem. C 114 (2010) 16481.
[17] J.C. Kim, J. Choi, Y.B. Lee, J.H. Hong, J.I. Lee, J.W. Yang, W.I. Lee, N.H. Hur, Chem. Commun. (2006) 5024–5026.
[18] M.L. Chen, K.Y. Cho, W.C. Oh, J. Mater. Sci. 45 (2010) 6611.
[19] L.R. Hou, C.Z. Yuan, Y. Peng, J. Hazard. Mater. B 139 (2007) 310.
[20] Y.X. Yu, D.S. Xu, Appl. Catal. B: Environ. 73 (2007) 166.
[21] M. Shang, W.Z. Wang, L. Zhang, S.M. Sun, L. Wang, L. Zhou, J. Phys. Chem. C 113 (33) (2009) 14727.
[22] K. Uchida, A. Ayame, Surf. Sci. 357–358 (1996) 170.
[23] H.Y. Ma, T. Dong, F.P. Wang, W. Zhang, B.B. Zhou, Electrochim. Acta 51 (2006) 4965.
[24] W.J. Ren, Z.H. Ai, F.L. Jia, L.Z. Zhang, X.X. Fan, Z.G. Zou, Appl. Catal. B. 69 (2007) 138.
[25] Z. Song, J. Hrbek, R. Osgood, Nano Lett. 5 (2005) 1327.
[26] C.H. Chen, Y.H. Liang, W.D. Zhang, J. Alloys Compd. 501 (2010) 168.
[27] X.S. Peng, G.W. Meng, J. Zhang, L.X. Zhao, J. Phys. D: Appl. Phys. 34 (2001) 3224.
[28] F. Li, X. Li, M. Hou, K. Cheah, W. Choy, Appl. Catal. A: Gen. 285 (2005) 181.
[29] T.Y. Zhang, T. Oyama, A. Aoshima, H. Hidaka, J.C. Zhao, N. Serpone, J. Photochem. Photobiol. A: Chem. 140 (2001) 163.
[30] Y. Zhou, F. Krumeich, A. Heel, G.R. Patzke, Dalton Trans. 39 (2010) 6043.